

## Single-Crystalline 4H-SiC Micro Cantilevers with a High Quality Factor

Kohei Adachi<sup>1,\*</sup>, Naoki Watanabe<sup>1</sup>, Hajime Okamoto<sup>2</sup>, Hiroshi Yamaguchi<sup>2</sup>,  
Tsunenobu Kimoto<sup>1</sup>, and Jun Suda<sup>1</sup>

<sup>1</sup> Department of Electronic Science and Engineering, Kyoto University, A1-303  
Kyotodaigakukatsura Nishikyo-ku, Kyoto 615-8510, Japan

<sup>2</sup> NTT Basic Research Laboratories, NTT Corporation, 3-1 Morinosatowakamiya Atsugi,  
Kanagawa 243-0198, Japan

\* E-mail: [adachi@semicon.kuee.kyoto-u.ac.jp](mailto:adachi@semicon.kuee.kyoto-u.ac.jp) / Phone: +81-75-383-2302

### **Abstract**

Single-crystalline 4H-SiC micro cantilevers were fabricated by doping-type selective electrochemical etching of 4H-SiC. Using this method, n-type 4H-SiC cantilevers were fabricated on a p-type 4H-SiC substrate, and resonance characteristics of the fabricated 4H-SiC cantilevers were investigated under a vacuum condition. The resonant frequencies agreed very well with the results of numerical simulations. The maximum quality factor in first-mode resonance of the 4H-SiC cantilevers was 230,000. This is 10 times higher than the quality factor of conventional 3C-SiC cantilevers fabricated on an Si substrate.

*Keywords:* MEMS; Single-crystalline 4H-SiC; Cantilever; Quality factor; Resonator

Microelectromechanical systems (MEMS) resonators have been adopted in various sensor and actuator applications because of their high frequency and high sensitivity [1,2]. There are many applications that require structures capable of operating in harsh environments such as high temperatures, high pressures, and corrosive environments. Silicon carbide (SiC) is a material that meets these demands because of its chemical stability, high yield strength, and wide bandgap [3-5]. Moreover, SiC is a very useful material for high-frequency resonators because its Young's modulus (448 GPa) [4] is much larger than those of other semiconductor materials commonly used for MEMS devices such as Si (130 GPa) and GaAs (85 GPa) [6].

These attractive characteristics give advantages to SiC resonators, and many papers on cubic-polytype 3C-SiC [7,8] and poly-SiC MEMS [9] resonators have been published. These SiC resonators are fabricated on Si substrates. These structures are easy to be manufactured and can be integrated with other Si devices. On the other hand, there have been few papers on hexagonal-polytype 4H- or 6H-SiC MEMS structures which are made of homoepitaxial layers grown on single-crystalline 4H- or 6H-SiC substrates [10-12]. Single-crystalline 4H- or 6H-SiC has more advantage in MEMS devices intended for use in harsh environments than 3C-SiC/Si or poly-SiC/Si because they do not use Si substrates. Si becomes conductive over 200°C resulting in leakage current via substrate and yield strength of Si declines over 450°C [3], which may limit range of mechanical operation. Furthermore, it is expected that 4H- or 6H-SiC MEMS can show superior resonance characteristics because of their high crystalline quality. However, these resonance characteristics have not been investigated in detail.

In this paper, we fabricated 4H-SiC cantilevers and measured their resonance characteristics. In addition, 3C-SiC cantilevers with the same dimensions as the 4H-SiC

cantilevers were fabricated on an Si substrate to compare their resonance characteristics.

Fig. 1 shows the fabrication process of single-crystalline 4H-SiC cantilevers. First, a 1- $\mu\text{m}$ -thick n-type 4H-SiC layer was grown on a p-type 4H-SiC substrate by chemical vapor deposition (CVD). (Fig. 1(a)) The doping concentration of the n-type SiC layer was  $4.5 \times 10^{18} \text{ cm}^{-3}$ . Next, an Ni layer was patterned by a photolithography lift-off process to form a mask for subsequent reactive ion etching (RIE). (Fig. 1(b)) Then, the n-type SiC was etched by capacitively coupled plasma RIE using  $\text{CF}_4$  and  $\text{O}_2$  gases. RIE was performed until the p-type SiC was exposed to the surface. (Fig. 1(c)) After the RIE process, we performed electrochemical (EC) etching, which can etch selectively on the basis of doping type [13]; by applying a positive voltage to the SiC, holes are supplied only at the interface between the p-type SiC and the solution, so that only p-type SiC is oxidized and etched. A Ti/Al/Ni layer was deposited on the back side, followed by rapid thermal annealing in an Ar atmosphere to form an ohmic contact. This metal layer was used as an electrode for EC etching. The EC etching was performed in 1 mol/l KOH solution at  $80^\circ\text{C}$  by applying a constant current to the p-type SiC for 12 min. The constant current source was set to 16 mA, which corresponds to a current density at the interface between the SiC and the KOH solution of  $3.3 \text{ mA/mm}^2$ . Under these conditions, the side-etching width of the substrate was about  $35 \mu\text{m}$  and the etched depth was about  $18 \mu\text{m}$ .

P-type SiC was selectively etched by EC etching, but the p-type SiC underneath the n-type SiC cantilevers was not completely etched, i.e., porous SiC remained in these areas, as shown in Fig. 1(d). Then, thermal oxidation was performed for 2.5 hours at  $1150^\circ\text{C}$  to remove the porous SiC, because it had a very large surface area; thus it was easily oxidized [14]. After the oxidation, the resulting  $\text{SiO}_2$  was removed using an HF

solution. In these processes, the porous SiC was completely removed, and the thickness of the SiC cantilevers was decreased from 1  $\mu\text{m}$  to about 900 nm. (Fig. 1(e)) Fig. 1(f) shows an SEM image of a fabricated 4H-SiC cantilever.

3C-SiC grown on an Si substrate by CVD was provided by HOYA corp [15]. 3C-SiC was patterned in the same way as the 4H-SiC by photolithography and RIE. Then, we used a 47wt% HF, 69wt% HNO<sub>3</sub>, and 99.7wt% CH<sub>3</sub>COOH solution with a volume ratio of 1:2:1 to selectively etch the Si.

The dimensions of the fabricated cantilevers were as follows. The width was 15  $\mu\text{m}$ . The lengths ranged from 80 to 140  $\mu\text{m}$ . The thickness of the 4H-SiC cantilevers was about 900 nm, while that of the 3C-SiC cantilevers was 1  $\mu\text{m}$ .

The resonance characteristics were measured as follows. Fabricated cantilevers were mounted on piezoceramic (lead zirconium titanate, PZT) actuators and placed in a vacuum chamber with a small window, which allowed optical access to the sample. The pressure in the chamber was 1.5 mTorr. The cantilevers were vibrated by applying a sinusoidal voltage to the PZT actuator while the frequency was swept. The resonance characteristics were measured by illuminating a laser light onto the center of the free-standing part of the cantilevers and detecting the reflected light with a laser Doppler vibrometer and a network analyzer. We measured the resonance characteristics in the frequency range below 1.5 MHz, in which the PZT actuator doesn't resonate.

Before performing more detailed characterizations, we changed the amplitude of the sinusoidal voltage from 0.2 to 20 mV<sub>RMS</sub> and measured the resonance characteristics. We confirmed that there was no dependence on either the resonant frequency or quality factor ( $Q$ ) of the cantilevers; therefore, the resonance characteristics responded linearly to the amplitude of the applied voltage in this region. All data shown in this paper were

obtained at an amplitude of 1 mV<sub>RMS</sub>.

In our measurements, two sharp resonance peaks corresponding to first- and second-mode resonance were clearly observed. Fig. 2 shows these resonant frequencies for 4H-SiC cantilevers of various lengths. The first- and second-mode resonant frequencies are shown by filled and open circles, respectively. We performed numerical simulations of the resonance characteristics of these cantilevers using the finite element method. The physical properties of the SiC used in these simulations were as follows. The density was 3.22 g/cm<sup>3</sup> and the Young's modulus was 448 GPa [4]. The first- and second-mode resonant frequencies obtained by the simulation are shown in Fig. 2 by two types of crosses. The first- and second-mode experimental resonant frequencies both agreed very well with the simulation results. The differences between experimental resonant frequencies and the simulation results are only 3% in average.

The same measurements and simulations were performed for 3C-SiC cantilevers. The experimental resonant frequencies of the 3C-SiC cantilevers also agreed with the simulation results. The resonant frequencies of the 3C-SiC cantilevers were about 10% higher than those of the 4H-SiC cantilevers because the 3C-SiC cantilevers were thicker than the 4H-SiC cantilevers.

Fig. 3 shows first-mode resonant spectra of 100- $\mu$ m-long 4H- and 3C-SiC cantilevers. The full-width at half-maximum (FWHM) of this 4H-SiC cantilever was 0.64 Hz, while that of the 3C-SiC cantilever was 8.6 Hz.  $Q$  was calculated as  $Q=f/\Delta f$ , where  $f$  is the resonant frequency and  $\Delta f$  is the FWHM.  $Q$  of the 4H-SiC was 230,000, and that of the 3C-SiC was 18,000.

Fig. 4 shows  $Q$  in first-mode resonance for cantilevers of various lengths.  $Q$  of all 4H-SiC cantilevers was nearly 200,000, while  $Q$  of the 3C-SiC cantilevers was nearly

20,000. Enderling *et al.* reported  $Q$  of a 3C-SiC cantilever in vacuum condition to be 14,755 [16], and  $Q$  of our 3C-SiC cantilevers was similar to this reported value.  $Q$  of 4H-SiC cantilevers was 10 times that of 3C-SiC. This shows that the energy dissipation of 4H-SiC cantilevers is much smaller than that of 3C-SiC.

The energy dissipation characteristics were discussed by Hosaka *et al.* and categorized as air damping, internal friction, and support loss [17]. We performed measurements under various air pressures to analyze the air damping loss. Fig. 5 shows  $Q$  of our SiC cantilevers in various pressures.  $Q$  of our cantilevers is independent of air pressure below 1.5 mTorr for 4H-SiC and 10 mTorr for 3C-SiC, and thus air damping can be neglected at 1.5 mTorr where above measurements were performed. Under the atmospheric pressure,  $Q$  of 4H-SiC and 3C-SiC cantilevers is similar; in this region, air damping loss is dominant.  $Q$  of 3C-SiC cantilevers is slightly higher. This is due to gap length between cantilevers and substrates. The gap of 4H-SiC is smaller, resulting in stronger air damping.

In 3C-SiC cantilevers, the dominant mechanism of energy dissipation is expected to be either internal friction or support loss. 3C-SiC films have a large number of defects such as stacking faults and dislocations, whose density is about  $2 \times 10^9 \text{ cm}^{-2}$ , because they are heteroepitaxially grown on Si substrates with a large lattice mismatch (20%) [15]. Defects in crystals are one of the sources of internal friction and can lead to energy dissipation. On the other hand, support loss is generated by the friction between connected surfaces. 3C-SiC cantilevers were fabricated on an Si substrate, which is a different material from the cantilevers; therefore, support loss cannot be neglected. Support loss decreases with increasing cantilever length, which means that  $Q$  increases with increasing cantilever length. In Fig. 4, long 3C-SiC cantilevers have a slightly

higher  $Q$  than short cantilevers.

4H-SiC cantilevers were fabricated on a high-quality 4H-SiC substrate (dislocation density  $< 10^4 \text{ cm}^{-2}$ ). Homoepitaxially-grown 4H-SiC films have significantly fewer defects than 3C-SiC films, and the internal friction is expected to be much lower. Furthermore,  $Q$  of 4H-SiC cantilevers is independent of cantilever length. This shows that 4H-SiC cantilevers are not influenced by support loss. 4H-SiC resonators were fabricated with only 4H-SiC, including the support, and thus, support loss is expected to be very small. These results clearly suggest that 4H-SiC is an ideal material for high- $Q$  resonators.

In summary, we fabricated single-crystalline 4H-SiC cantilevers on a 4H-SiC substrate by selective etching of p-type SiC using electrochemical etching and thermal oxidation. The maximum  $Q$  of the 4H-SiC cantilevers was 230,000.  $Q$  of the 4H-SiC cantilevers was 10 times that of conventional 3C-SiC cantilevers fabricated on an Si substrate. Although the fabrication process of 4H-SiC MEMS is more difficult than that of 3C-SiC/Si MEMS, their very high  $Q$  makes 4H-SiC MEMS very attractive for high-sensitivity sensors.

## References

- [1] J.W. Judy, Microelectromechanical systems (MEMS): fabrication, design and applications, *Smart Mater. Struct.* **10** (2001) 1115-1134.
- [2] P.S. Waggoner, H.G. Craighead, Micro- and nanomechanical sensors for environmental, chemical, and biological detection, *Lab Chip* **7** (2007) 1238-1255.
- [3] T. Suzuki, I. Yonenaga, H.O.K. Kirchner, Yield Strength of Diamond, *Phys. Rev. Lett.* **75** (1995) 3470-3472.
- [4] M. Mehregany, C.A.Zorman, N. Rajan, C.H. Wu, Silicon carbide MEMS for harsh environments, *Proc. IEEE* **86** (1998) 1594-1610.
- [5] P.M. Sarro, Silicon carbide as a new MEMS technology, *Sens. Actuators A* **82** (2000) 210-218.
- [6] W.A. Brantley, Calculated elastic constants for stress problems associated with semiconductor devices, *J. Appl. Phys.* **44** (1973) 534-535.
- [7] K. Brueckner, V. Cimalla, F. Niebelschutz, R. Stephan, K. Tonisch, O. Ambacher, M.A. Hein, Strain- and pressure-dependent RF response of microelectromechanical resonators for sensing applications, *J. Micromech. Microeng.* **17** (2007) 2016-2023.
- [8] M. Placidi, P. Godignon, N. Mestres, G. Abadal, G. Ferro, A. Leycuras, T. Chassagne, Fabrication of monocrystalline 3C-SiC resonators for MHz frequency sensors applications, *Sens. Actuators B* **133** (2008) 276-280.
- [9] S. Roy, R.G. DeAnna, C.A. Zorman, M. Mehregany, Fabrication and characterization of polycrystalline SiC resonators, *IEEE Trans. Electron Devices* **49** (2002) 2323-2332.
- [10] J. Suda, N. Watanabe, K. Fukunaga, T. Kimoto, Electrostatic-actuated suspended ribbon structure fabricated in single-crystalline SiC by selective photoelectrochemical

etching, *Jpn. J. Appl. Phys.* **48** (2009) 111101-1-4.

[11] F. Zhao, M.M. Islam, Fabrication of single-crystal silicon carbide MEMS/NEMS for bio-sensing and harsh environment, *Proceedings of 2011 IEEE 24th International Conference on MEMS* (2011) 261-263.

[12] M.M. Islam, C.F. Huang, F. Zhao, Single-crystal SiC resonators by photoelectrochemical etching, *Mater. Sci. Forum* **717-720** (2012) 529-532.

[13] S. Rysy, H. Sadowski, R. Helbig, Electrochemical etching of silicon carbide, *J. Solid State Electrochem.* **3** (1999) 437-445.

[14] M.W. Shin, J.G. Son, Study on the photoelectrochemical etching process of semiconducting 6H-SiC wafer, *Mater. Sci. Eng. B* **95** (2002) 191-194.

[15] H. Nagasawa, K. Yagi, 3C-SiC single-crystal films grown on 6-inch Si substrates, *Phys. Status Solidi B* **202** (1997) 335-358.

[16] S. Enderling, J. Hedley, L. Jiang, R. Cheung, C. Zorman, M. Mehregany, and A.J. Walton, Characterization of frequency tuning using focused ion beam platinum deposition, *J. Micromech. Microeng.* **17** (2007) 213-219.

[17] H. Hosaka, K. Itao, S. Kuroda, Evaluation of energy dissipation mechanisms in vibrational microactuators, *Proceedings of the MEMS '94* (1994) 193-198.

## Figure Captions

Fig. 1. Fabrication process and an SEM image of a 4H-SiC cantilever. This structure consists of an n-type SiC cantilever and a p-type SiC substrate.

Fig. 2. Resonant frequencies of 4H-SiC cantilevers of various lengths and schematic illustrations of first- and second-mode resonance of cantilevers.

Fig. 3. Spectrum of (a) 4H-SiC and (b) 3C-SiC cantilevers.  $L$  and  $f$  are the length and resonant frequency of these cantilevers, respectively.

Fig. 4.  $Q$  in first-mode resonance for cantilevers of various lengths.  $Q$  of the 4H-SiC cantilevers was 10 times that of the 3C-SiC cantilevers.

Fig. 5.  $Q$  in first-mode resonance for cantilevers in various air pressures.  $Q$  of the 4H-SiC cantilevers was independent of air pressure below 1.5 mTorr and that of 3C-SiC cantilevers was independent below 10 mTorr.

Fig. 1

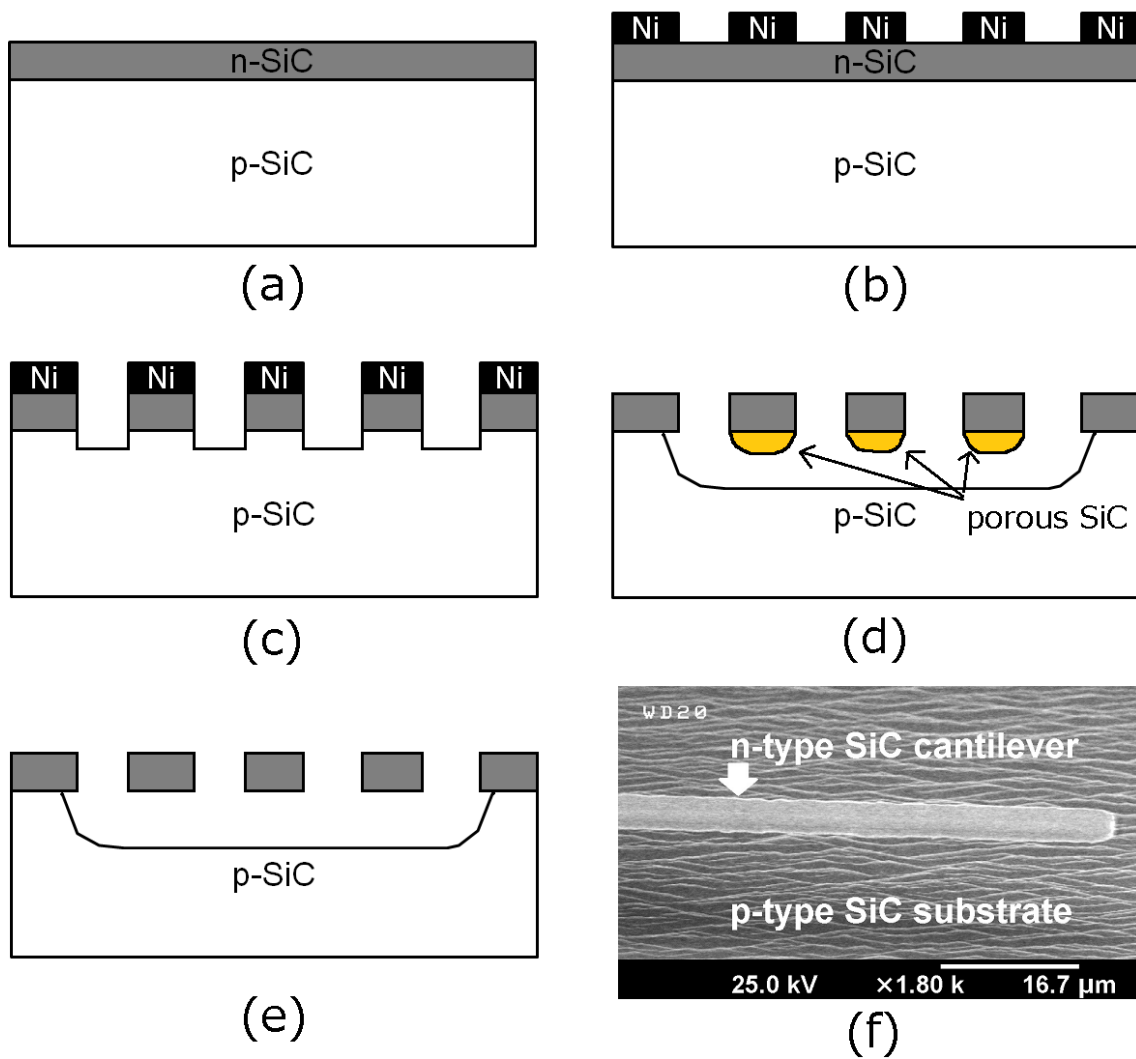


Fig. 2

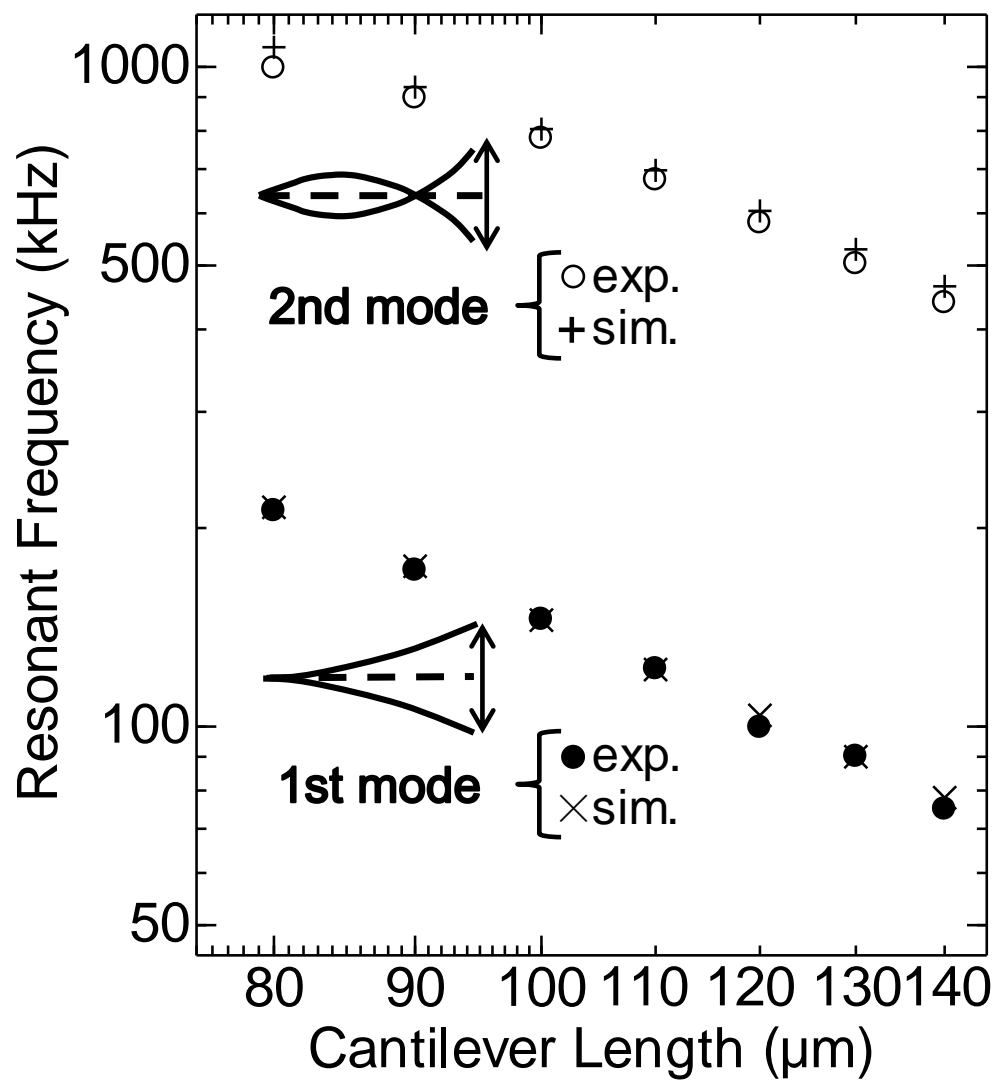


Fig. 3 (a)

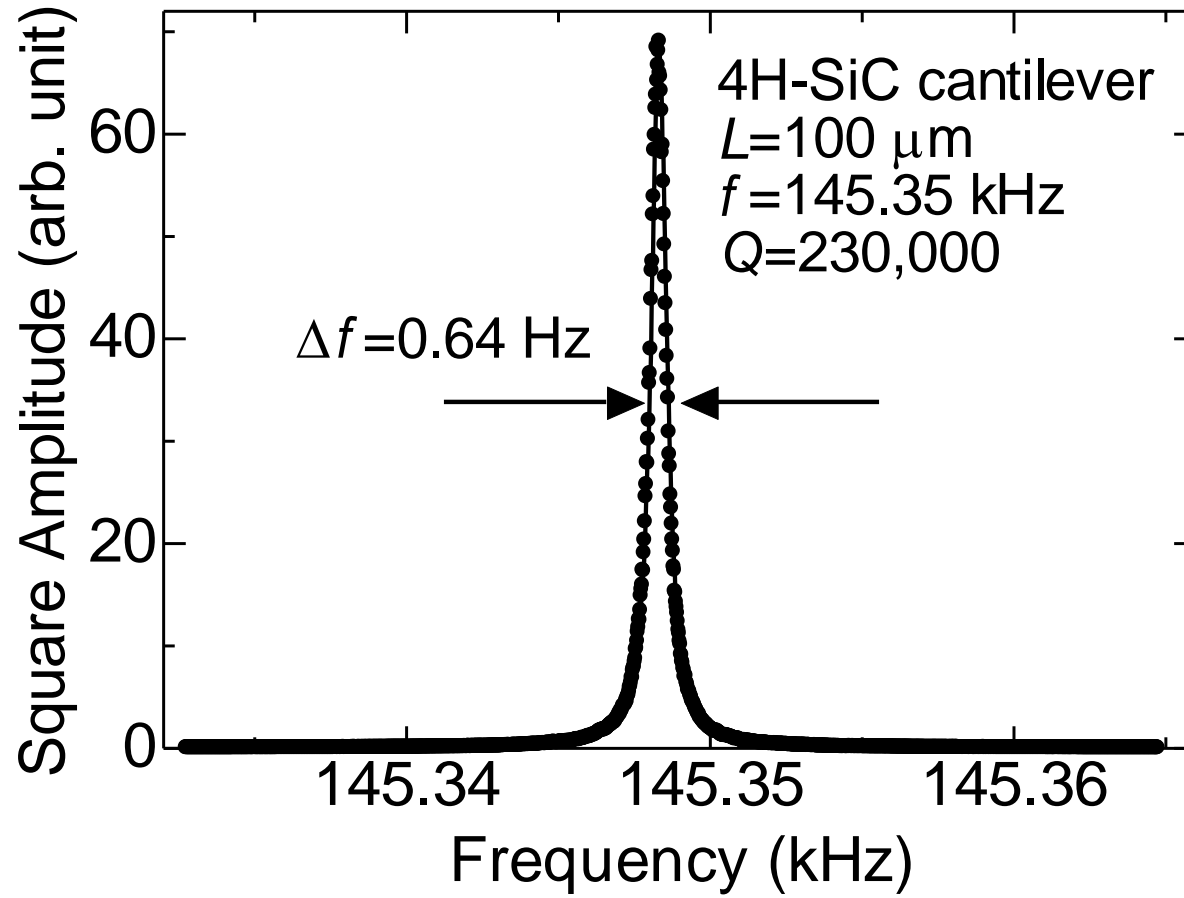


Fig. 3 (b)

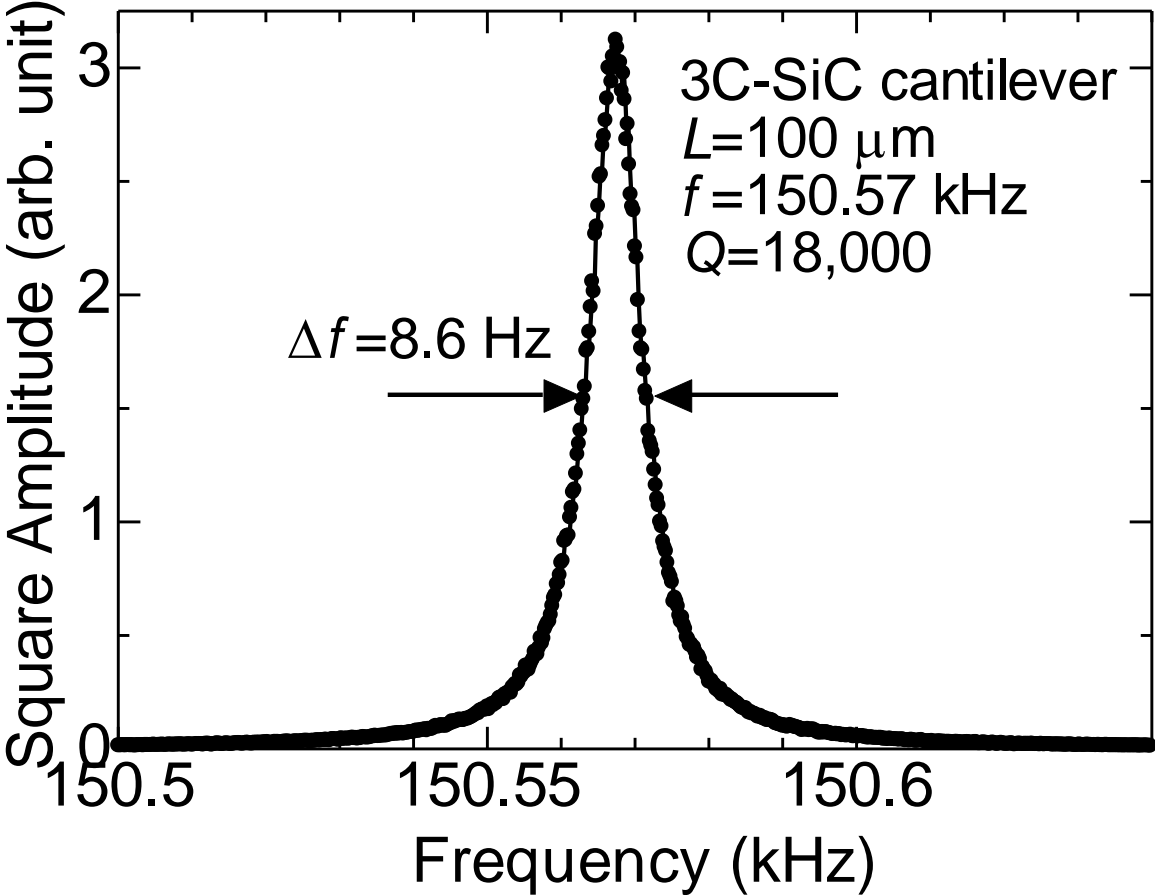


Fig. 4

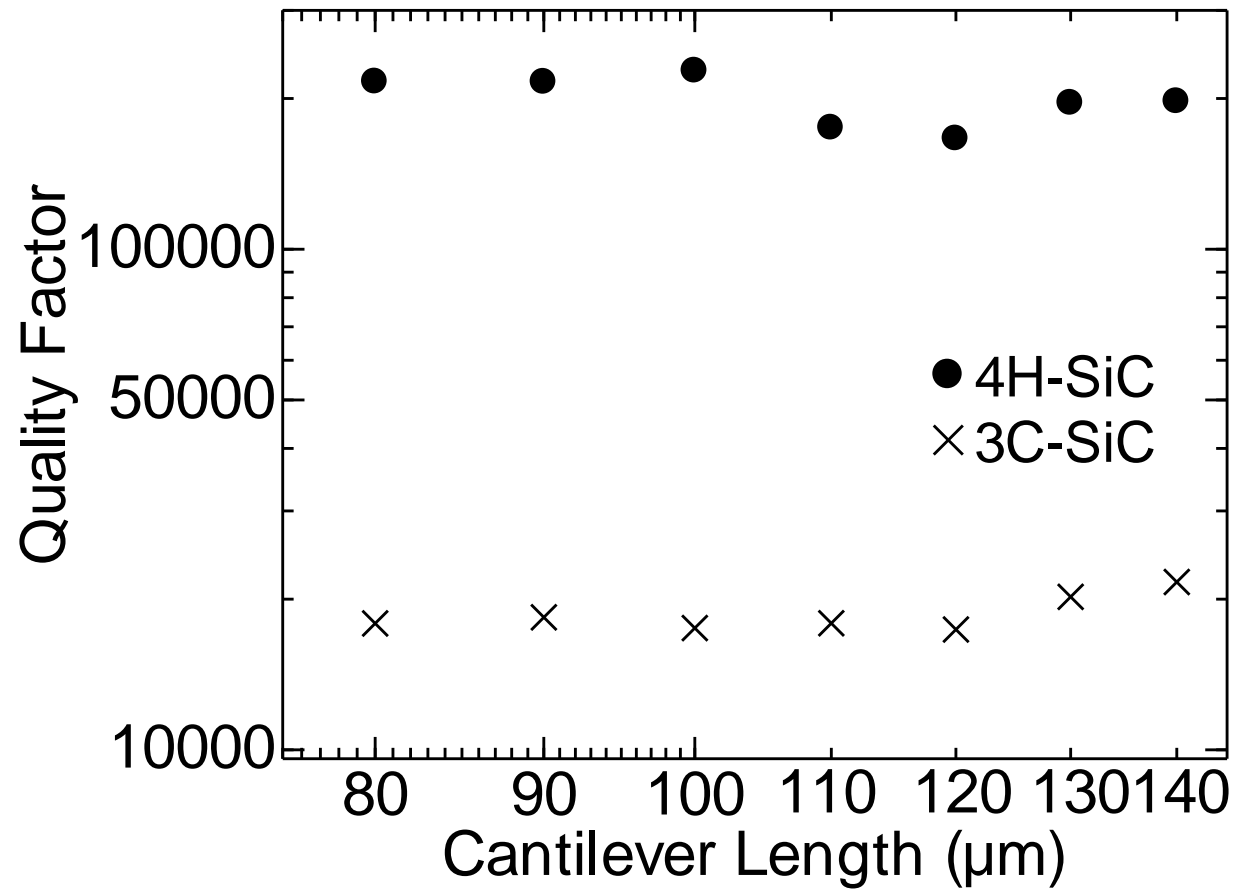


Fig. 5

